Dark Sector first results at Belle II

Marcello Campajola on behalf of the Belle II collaboration
Dip. di Fisica 'E. Pancini', Univ. degli Studi di Napoli 'Federico II', Napoli, Italy
E-mail: marcello.campajola@na.infn.it, marcello.campajola@unina.it

January 2021

Abstract.
Understanding the nature of dark matter is one of the most exciting challenges in fundamental physics nowadays, requiring the synergy of different search techniques, as well as theoretical inputs. An interesting direction for the investigation of dark matter is the one offered by the B-factories. The Belle II experiment at the SuperKEKB energy-asymmetric e^+e^- collider is a substantial upgrade of the B-factory facility at the Japanese KEK laboratory. With a machine design luminosity of $6 \times 10^{35}\,\mathrm{cm}^{-2}\mathrm{s}^{-1}$, the Belle II experiment aims to record 50 ab^{-1} of data: a factor of 50 more than its predecessor. Thanks to this large data-sample and by using dedicated triggers the Belle II experiment is expected to explore dark sector candidates with an unprecedented sensitivity in a mass range up to 10 GeV/c^2. During 2018, the machine has completed a commissioning run, recording a data-sample corresponding to an integrated luminosity of about 0.5 fb^{-1}, while main operations started on March 2019 with an almost complete detector. An integrated luminosity of $\sim 90\,\mathrm{fb}^{-1}$ has been collected so far. These early data sets offer already the possibility to search for a large variety of dark sector particles in the GeV mass range. This paper reviews the status of the dark-sector searches at Belle II, with a focus on the first obtained results, and the discovery potential with the data-set available in the short term.

Keywords: Low-mass Dark Matter, Dark Sector, Dark Photon, Axion-Like Particles, Belle II, B–factories.

1. Introduction

A variety of observations, from galaxies to larger scale structures in the Universe, suggests the existence of the *Dark Matter* (DM), consisting of particles which do not interact through strong or electromagnetic forces. It has been estimated that DM accounts for ∼27% of the total energy density of the Universe and for about 85% of its matter density [1]. However, the fundamental nature of the DM is still a puzzling mystery, providing one of the most important open problems in particle and astroparticle physics nowadays. It cannot be incorporated within the Standard Model (SM) of particles, and its understanding requires, in most of the theoretical scenarios, the introduction of new degrees of freedom.

Although dark matter has traditionally been associated with heavy candidates, WIPMs for example, a class of lighter particles remains a well motivated alternative. Many models have been recently proposed to accommodate light dark matter, ranging from minimal scenarios including a single dark matter particle to the case of an entire structure decoupled from SM, a so called *Hidden* or *Dark Sector*. This Dark Sector may contain new light dark matter (LDM) particles well below the weak scale, that interact feebly with ordinary matter, so that they could easily have escaped past experimental searches. The connection between SM and the dark sector is usually made through a 'mediator', i.e., a particle which possesses both Standard Model and dark sector quantum numbers, and interacts with SM particles either directly or indirectly through loop diagrams or mixing. Depending on the mediator properties, several scenarios are possible, and a few categories of models are available [2]. Other than predicting the observed DM abundance, the introduction of dark sector particles could explain other features: it could be invoked to explain the antimatter excess in the cosmic rays [3–5] as well as some SM anomalies, including the discrepancy between the calculated and the measured anomalous magnetic moment of the muon [6].

In recent times, DM searches at colliders have received much attention. To date, most of the focus has been on searches with high-energy colliders such as LEP, Tevatron and LHC [7]. Such experiments are ideally suited to probing weak scale DM. In contrast, low-energy e^+e^- colliders such as B-factories, as they operate at a much lower center-of-mass energy, have higer sensitivity to light DM with low-mass mediators [8].

This paper will give an overview of the dark sector searches performed or capable of being performed at the Belle II experiment at the Japanese KEK laboratory. The expected large data-set and the clean e^+e^- environment, combined with a trigger specifically designed to have high efficiency for low-multiplicity events, will enable Belle II to explore dark sector physics with unprecedented precision in a mass range up to $\sim$10 GeV/c^2. The research program is broad and foresees to significantly extend the range of parameters covered by previous low-energy e^+e^- experiments, namely BaBar, Belle, BESIII and KLOE. Here, we will focus on the first results obtained with the early data-sets collected so far and on the discovery potential of the data-set which will be shortly available.

2. Status of the Belle II experiment

Belle II is a full upgrade of the Belle experiment operating at the KEK laboratory (Japan). The Belle II experiment is located at the interaction region of the SuperKEKB machine [9], an e^+e^- energy-asymmetric collider that operates at a centre-of-mass (CM) energy of 10.58 GeV, which corresponds to the $\Upsilon(4S)$ resonance mass. As it decays mostly into a pair of B mesons, Belle II and SuperKEKB are called a B–factory experiment. Specifically, they are a second generation B-factory, where both the detector and the machine have undergone a renewal compared to the predecessor experiment (Belle at KEKB). The higher beam currents, the smaller interaction

region and the application of the large crossing angle nano-beams scheme [10] will allow SuperKEKB to provide a significant increase in the instantaneous luminosity with respect to KEKB. Values of $6 \times 10^{35}\text{cm}^{-2}\text{s}^{-1}$ are expected soon. Belle II inherits the design of the Belle detector [11] with major improvements in all of the subsystems. It consists of different layers of sub-detectors arranged in a cylindrical geometry around the interaction region. The innermost sub-detector is the silicon vertex detectors (VXD), which is surrounded by the main tracking device (CDC) made off a large helium-based small-cell drift chamber. A particle identification system follows, including an imaging time-of-propagation (TOP) detector in the barrel region and an aerogel ring imaging Cherenkov (ARICH) detector in the forward endcap region. Following, the electromagnetic calorimeter (ECL), composed of 8736 CsI(Tl) crystals and the outermost detector (KLM) responsible for K_L and muon reconstruction. A superconducting solenoid, situated outside the calorimeter, provides a 1.5 T magnetic field. The detector is described in more details in Ref. [12].

The final integrated luminosity goal of SuperKEKB and Belle II is 50 ab^{-1} by 2030, with a large portion of the data collected at the nominal collision energy ($\sqrt{s}$ = 10.58 GeV). This high integrated luminosity offers possibilities for a wide physics program. While the primary purpose of Belle II is to study the properties of B-mesons, the experiment is ideally suited for a wide range of new-physics searches, including dark sector physics. Indeed, because of the simple and clean initial state, Belle II is very sensitive to final states with invisible particles, thus having excellent potential for searches in the dark sector. In addition, a major upgrade with respect to previous B–factories experiments comes from new triggers specifically designed to have high efficiency for events with a low number of particles in the final state: most relevant is the newly designed single-photon trigger.

The experiment performed the first data taking runs for physics analysis during 2018. During this period, the experiment worked with a partially installed vertex detector at a reduced instantaneous luminosity for commissioning purposes. An integrated luminosity of approximately 0.5 fb^{-1} was collected [13]. In the early 2019, Belle II started the main operations with a near-complete detector and has collected approximately 90 fb^{-1} of data so far.

3. Axion-like Particles

With the expression Axion-like particles (ALPs) one refers to a class of hypothetical pseudo-scalar ($J^P = 0^-$) particles that occur in many extensions of the standard model [14]. Differently from axions, introduced to preserve some of the QCD properties [15], the mass and the coupling of ALPs are independent. ALPs are frequently involved as interaction mediators between SM and yet undiscovered DM particles [16].

ALPs can couple to both SM bosons and fermions. Cases where they predominantly couple to $\gamma\gamma$, γZ^0, and $Z^0 Z^0$ are experimentally much less constrained than those that couple to gluons or fermions. Among the former, the most accessible at a low energy

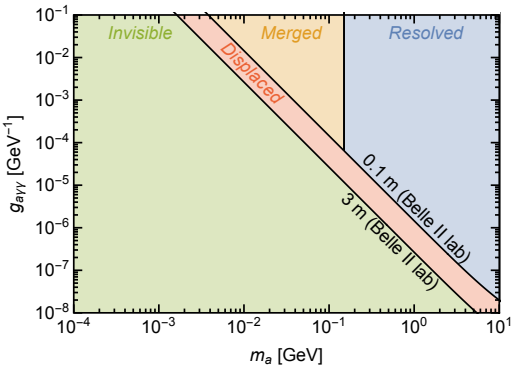

Figure 1: Signatures of the ALP decay into two photons with the Belle II detector, as a function of the ALP mass m$_a$ and of the coupling constant $g_{a\gamma\gamma}$ [16].

e^+e^- collider is the case where ALPs couple to photons. In particular, there are two different production processes of interest: ALP–strahlung $e^+e^- \to \gamma^* \to \gamma\, a$ and photon-photon fusion $e^+e^- \to e^+e^-a$.

3.1. Two-photon decay

Among the first results obtained by Belle II is the search for ALPs produced by the ALP–strahlung process, with the following decay into two photons. Unless m_a is close to $\sqrt{s}$, ALP production via photon fusion typically dominates over ALP-strahlung. However, the latter is ALPs much harder to detect experimentally: ALPs carry little energy thus decaying into relatively soft photons, which results in large QED backgrounds [16]. For this search, it was assumed a predominant coupling to photons with strength $g_{a\gamma\gamma}$, and a negligible coupling strength $g_{a\gamma Z}$ to a photon and a Z^0 boson, so that $BR(a \to \gamma\gamma) = 100\%$.

The experimental signature of the decays into two photons is determined by m_a and $g_{a\gamma\gamma}$, as illustrated in Figure 1. They affect both the ALP decay length and the opening angle between the photons [16]. For high ALP masses, the small boost leads to a wide opening angle of the decay photons, thus to a final state with three detectable photons, denoted as *Resolved* in Figure 1. For small ALP masses, the higher boost leads to a decreased opening angle of the decay photons that cannot be resolved due to the limited spatial resolution of the electromagnetic calorimeter, for $m_a < 200\,\mathrm{MeV}$, denoted as *Merged*. *Invisible* denotes the case where the ALP is long-lived, decaying outside of the detector volume. Here, only one photon can be detected. A further case, denoted by *Displaced*, represents the case when the ALP decay is displaced from the interaction point but still inside the Belle II detector.

Belle II searched for an ALP decay into two photons produced with the ALP–strahlung process ($e^+e^- \to \gamma\, a$, $a \to \gamma\gamma$) over a mass range $0.2 < m_a < 9.7$ GeV/c^2 in the resolved three-photon final state [17]. The entire data-set collected during 2018

was used for this analysis. A subset of data was used to validate the selection and then discarded; the remaining data-set used for this search corresponds to an integrated luminosity of 0.445 pb^{-1}. The final state consists of three photons, with two of them peaking at the ALP mass, while the recoiling one being a mono-energetic photon in the CM frame of energy $E^{\mathrm{CM}}_{\mathrm{rec}_\gamma} = (s - m_a^2)/2\sqrt{s}$. The signal signature is a narrow peak in the squared mass distribution of the recoiling system against the mono-energetic photon $M^2_{\mathrm{rec}} = s - 2\sqrt{s}E^{\mathrm{CM}}_{\mathrm{rec}_\gamma}$, or in the squared-invariant-mass distribution of the two decay photons $M^2_{\gamma\gamma}$.

The dominant SM background comes from the QED process $e^+e^- \to \gamma\gamma\gamma$. A smaller background source arise especially for small ALP masses from $e^+e^- \to \gamma\gamma$ with a third photon candidate coming from beam-induced backgrounds, or in the case where one of the two photons converts into an electron-positron pair outside of the tracking detectors, resulting in both electron and positron identified as photons. An additional contribution comes from $e^+e^- \to e^+e^-\gamma$ due to tracking inefficiencies. The analysis selection requires that the three-photon candidates have a combined invariant mass close to the center-of-mass energy, and are reconstructed in time with each other. After the final selection the expected background distributions are dominated by $e^+e^- \to \gamma\gamma\gamma$, with a small contribution from $e^+e^- \to e^+e^-\gamma$. A mass scan technique has been adopted to search for peaks as a function of m_a by performing a series of independent binned maximum-likelihood fits. Fits have been performed on the invariant mass $M_{\gamma\gamma}$ in the ALP low-mass region, while on the recoil spectrum $M^2_{\mathrm{rec}_\gamma}$ for the higher part, since the resolution of $M_{\gamma\gamma}$ worsens with increasing m_a, while that of $M^2_{\mathrm{rec}_\gamma}$ improves.

Both the analysis selection and the statistical interpretation procedures have been optimized on Monte Carlo simulation prior to examining data. No significant excess of events consistent with an ALP signal has been observed in data. Thus 95% confidence level (C.L.) upper limits on the cross section as a function of m_a using a one-sided frequentist profile-likelihood method have been computed (Figure 2a), and then converted in terms of the $g_{a\gamma\gamma}$ coupling. These latter limits are shown in Figure 2b together with the existing constraints from previous experiments. These limits are more restrictive than existing limits for $0.2 < m_a < 1$ $\mathrm{GeV/c^2}$. In a future update of the analysis with an increased luminosity, Belle II is expected to improve the sensitivity to $g_{a\gamma\gamma}$ by more than one order of magnitude [16].

3.2. Invisible decay

In this section, we will extend the above discussion and consider the case of ALPs coupled to DM particles χ. In such a scenario, provided the DM is sufficiently light ($m_\chi < 1/2\, m_a$), the ALP has an invisible decay mode $a \to \chi\bar{\chi}$. Thus one can look at the ALP invisible decay produced with the ALP–strahlung process ($e^+e^- \to \gamma\, a$, $a \to$ invisible). Such a signature is of particular interest, since the limits obtained with the two-photon decay search assume that the dominant decays of the a is to visible SM particles, but this is not valid anymore if there are low-mass invisible degrees of freedom.

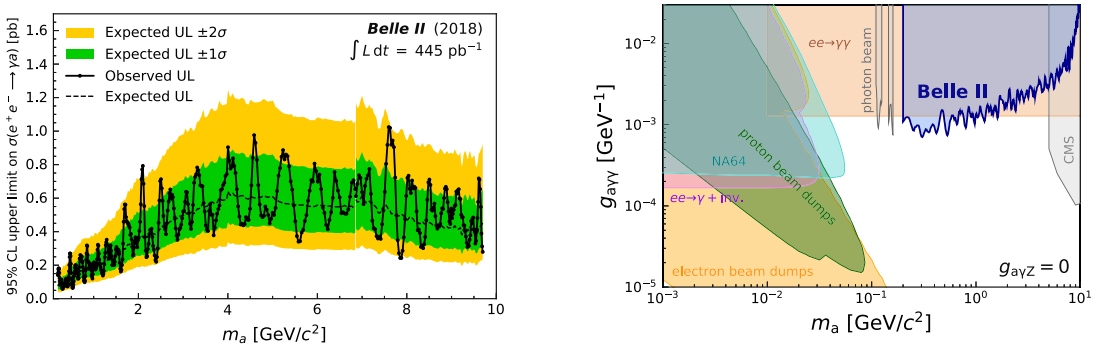

(a) (b)

Figure 2: Results for the $e^+e^- \to \gamma\, a$, $a \to \gamma\gamma$ search performed with the 2018 data-set (455 pb^{-1}) [17]. (a) Expected and observed upper limits (95% C.L.) on the ALP cross section σ_a. (b) Upper limit (95% C.L.) on the ALP-photon coupling $g_{a\gamma\gamma}$ from this analysis and previous constraints.

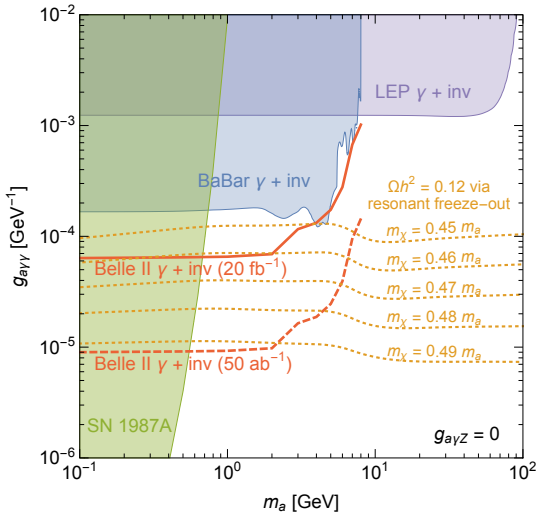

Figure 3: Expected upper limits (90% C.L.) on $g_{a\gamma\gamma}$ for the process $e^+e^- \to \gamma\, a$, $a \to \chi\bar{\chi}$, compared to the parameter region where one can reproduce the observed DM relic abundance via resonant annihilation of DM into photons [16].

The final state consists of a single mono-energetic photon in the CM frame of energy $E^{\rm CM}_{{\rm rec}_\gamma} = (s - m_a^2)/2\sqrt{s}$. This search has the same experimental signature of the dark photon decays into DM, described below. However, the angular distribution of the recoil photon is less peaked at small angles than the ISR photon in the radiative dark photon production. Using the the same event selection as for the mono-photon dark photon search, the expected sensitivity to $g_{a\gamma\gamma}$ via the process $e^+e^- \to \gamma\, a$, $a \to \chi\bar{\chi}$ has been computed for 20 fb^{-1} and 50 ab^{-1} (Figure 3).

4. Z' ($L_\mu - L_\tau$ model)

An interesting scenario beyond SM is the one based on the $L_\mu - L_\tau$ model, which gauges the difference of the leptonic muon and tau number. As a result, a new gauge boson Z' is introduced that feebly couples to the 2$^{\text{nd}}$ and 3$^{\text{rd}}$ generation leptons with a new coupling constant indicated with g'. Such a boson does not couple with e and ν_e and thereby may have escaped existing searches [18, 19]. This model is of particular interest, being able to explain various phenomena not accounted for within the SM, i.e., dark matter abundance, the $(g-2)_\mu$ anomaly and anomalies in the $b \to s\mu^+\mu^-$ decays reported by the LHCb experiment.

At an e^+e^- collider the Z' would be produced in processes such as $e^+e^- \to \mu^+\mu^- Z'$ or $e^+e^- \to \tau^+\tau^- Z'$, thus being radiated from one of the final state muons ot taus and then eventually decaying either visibly into a muon or tau pair, or invisibly to neutrinos or dark matter. Related searches have been performed by the BABAR and CMS experiments for a Z' produced with a muon pair and decaying to muons [20, 21].

4.1. Invisible Decay

Belle II investigated for the first time the invisible decay topology $e^+e^- \to \mu^+\mu^- Z'$, $Z' \to$ invisible where the Z' is radiated from one of the two muons [22]. The final state consists of two opposite charged muon tracks coming from the interaction point plus missing energy. According to the $L_\mu - L_\tau$ model, the Z' decay branching ratio depends on the boson mass $m_{Z'}$ as follow: if $m_{Z'} < 2m_\mu$, the only possibility is the invisible decay to neutrinos and $BR(Z' \to \text{invisible}) = 1$. If $m_{Z'} > 2m_\tau$ both visible decays in muons and taus and the invisibile decay are allowed, thus $BR(Z' \to \text{invisible}) \sim 1/3$ [23]. However, if a kinematically accessible dark matter particle exists and if it is charged under $L_\mu - L_\tau$, due to the expected much stronger coupling relative to SM particles, the branching ratio of the invisible decay is enhanced to 1. Invisible decay topology is then a probe for the existence of new invisible particles.

This search has been performed by Belle II using the data collected during the 2018 pilot run. Due to the low-multiplicity trigger configuration usable for this search, only 0.276 fb^{-1} were available. The final state can be reconstructed by knowing the energy of the initial e^+e^- state and the properties of the muon tracks in the CM frame with a high accuracy. It is possible to define the recoil mass against the muon pair $M^2_{\text{rec}} = s + M^2_{\mu\mu} - 2\sqrt{s}E^{\text{CM}}_{\mu\mu}$, where $M^2_{\mu\mu}$ is the squared invariant mass of the muon pair and $E^{\text{CM}}_{\mu\mu}$ is the sum of the muon energies in the CM frame. In the case of signal events, 'recoil' quantities coincide with the Z' features; thus a peak in the M^2_{rec} distribution corresponding to the Z' mass is expected. The dominant backgrounds are SM final states with two tracks identified as muons and missing energy due to undetected particles. The primary backgrounds come from QED processes such as $e^+e^- \to \mu^+\mu^-(\gamma)$ with one or more photons not detected due to inefficiencies or being out of acceptance, $e^+e^- \to \tau^+\tau^-(\gamma)$ where missing momentum arises from neutrinos from both τ decays, and $e^+e^- \to e^+e^-\mu^+\mu^-$ with electrons out of acceptance.

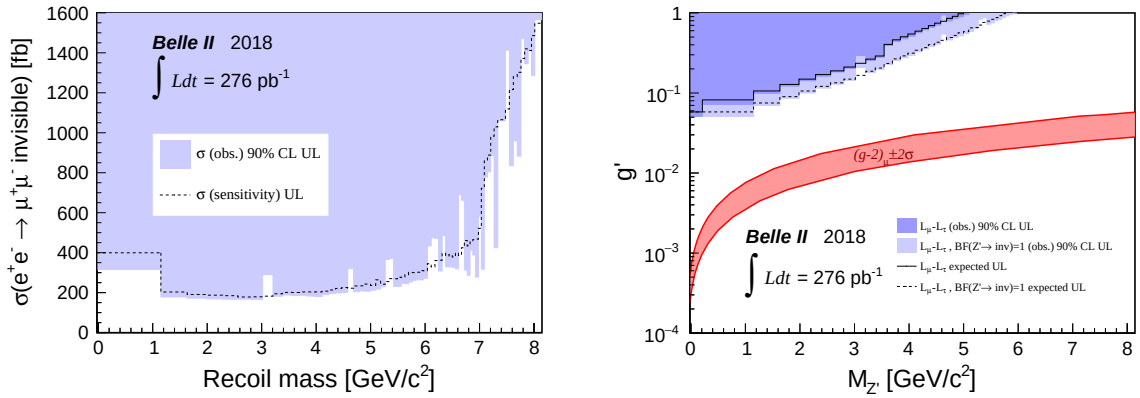

(a) (b)

Figure 4: Results for the $e^+e^- \to \mu^+\mu^- Z'$, $Z' \to$ invisible search performed with the 2018 data-set (276 pb^{-1}) [22]. (a) 90% C.L. upper limits on the cross section $\sigma(e^+e^- \to \mu^+\mu^- Z', Z' \to \text{invisible})$. The dashed line is the expected sensitivity. (b) 90% C.L. upper limits on coupling constant g'. Dark blue filled areas show the exclusion regions for g' at 90% C.L., assuming the branching ratio $BR(Z' \to \text{invisible})$ predicted by the $L_\mu - L_\tau$ model; light blue areas are for $BR(Z' \to \text{invisible}) = 1$. The solid and dashed lines are the expected sensitivities for the two hypotheses. The red band shows the region that could explain the muon anomalous magnetic moment $(g-2)_\mu \pm 2\sigma$.

The selection has been optimized using simulated events prior to examining data. After the final selection, almost all background sources with the exception of $e^+e^- \to e^+e^-\mu^+\mu^-$ are rejected. Control samples on data are used to check background rates predicted by simulation and to estimate correction factors and related uncertainties. The largest sources of systematic uncertainty result from poor agreement between data and Monte Carlo simulations and limited statistics of the control samples, which are expected to reduce as the data size will increase. A counting technique within mass windows with size equal to twice the recoil mass resolution has been performed. The final recoil mass spectrum is shown in Figure 4a, together with the expected background. No anomalies have been observed, with all results below 3σ local significance. The 90% credibility level (C.L.) upper limits on the cross section have been computed using a Bayesian procedure, and results have been translated into 90% C.L. upper limits on the coupling constant g'. This latter is shown in Figure 4b. Upper limits on the coupling constant in the range $[5 \times 10^{-2} - 1]$ have been set for $M_{Z'} \leq 6$ GeV/c^2.

Updates of the analysis are expected to improve the sensitivity to g' by more than one order of magnitude, already with the integrated luminosity achieved so far $\mathcal{O}(50\,\text{fb}^{-1})$. Thus, with the next data-sets there will be a serious possibility to exclude a good part of the region of the parameters able to explain the $(g-2)_\mu \pm 2\sigma$ anomaly.

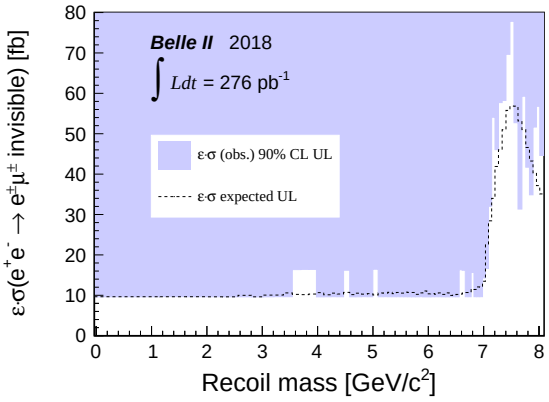

Figure 5: Results for the $e^+e^- \to e^\pm\mu^\mp Z'$, $Z' \to$ invisible search performed with the 2018 dataset (276 pb^{-1}) [22]: 90% C.L. upper limits on efficiency times cross section $\epsilon \times \sigma(e^+e^- \to e^\pm\mu^\mp \text{invisible})$ (light blue areas). The dashed line is the expected sensitivity.

5. Lepton Flavour Violating Z'

As an extension of the search for the invisibly decaying Z' in the process $e^+e^- \to \mu^+\mu^- Z'$, $Z' \to$ invisible, the existence of a Lepton Flavour Violating (LFV) Z' boson has been investigated. Specifically, the search focused on an invisibly decaying LFV Z' produced in the process $e^+e^- \to e^\pm\mu^\mp Z'$, $Z' \to$ invisible [22]. The experimental signature consists of two oppositely charged tracks with different flavours plus missing energy. The search for a LFV final state is expected to have a small SM background. A model-independent search has been performed for this channel, by using the same selection criteria of the above ($L_\mu - L_\tau$ model) Z' search, aside from the obvious requirement to have an electron instead of a muon in the final state. The only SM background contribution after the final selection is $e^+e^- \to \tau^+\tau^-(\gamma)$ with taus going to one-prong muon and one-prong electron. In case of signal events, a bump in the distribution of the mass recoiling against the $e\mu$ system is expected at the mass value of the LFV Z'.

This search has been performed with the 2018 data-set, which is the same as that used for the Z' search in the $L_\mu - L_\tau$ framework. Also in that case, no anomalies have been observed above 3σ local significance. Using a Bayesian procedure, model-independent 90% C.L. upper limits on the LFV Z' efficiency times cross section have been computed, as shown in Figure 5.

6. Dark Photon

One of the simplest ways to extend the SM is to includes a new gauge boson A', called *dark photon*, that mixes kinetically to the SM photon with a strength $\epsilon < 1$ [24, 25]. The mixing strength can be understood as the suppression factor relative to the coupling

with the electron charge e.

6.1. Radiative Processes

A simple way to search for a dark photon at an e^+e^- collider is in the initial state radiation (ISR) process $e^+e^- \to \gamma_{\rm ISR}\, A'$, whose cross section is proportional to $\epsilon^2\alpha^2/s$ where α is the electromagnetic coupling.

The decay modes of the dark photon depend on its mass and couplings, as well as on the particle spectrum of the dark sector. It can decay into SM final states $A' \to l^+l^-$ or $A' \to h^+h^-$ (l=leptons, h=hadrons) with an expected branching ratio equal to that of a virtual photon of mass $m_{A'}$. In such a scenario, the dark photon search proceeds by looking for a resonance in the invariant mass distribution of the reconstructed daughter particles. In the case of long-lived A', the decay can happen far from the production point, thus one expects the two-tracks vertex would be significantly displaced with respect to the interaction region.

If a sufficiently low mass dark matter state χ exists (such that $m\chi < 1/2\, m_{A'}$), one can assume that the dominant decay mode of the dark photon is into DM via $A' \to \chi\bar{\chi}$. Since the interaction probability of dark matter with the detector is negligible, this case is referred to as *invisible* decay (while the former case is referred to as *visible* decay). The experimental signature of the process $e^+e^- \to \gamma_{\rm ISR}\, A'$, $A' \to \chi\bar{\chi}$ would be only a mono–energetic ISR photon, accompanied by significant missing energy and momentum. In such a case, the energy of the ISR photon is related to the dark photon mass $m_{A'}$ through the relationship $E_\gamma = \frac{s-m^2_{A'}}{2\sqrt{s}}$. The search, then, occurs as a scan of the squared mass distribution of the recoiling system against the ISR photon.

Two recent searches by the BaBar experiments looked for the radiative production of the A' in both visible [22] and invisible final states [26].

6.1.1. Invisible Decay: Searches for dark photon in ISR process are expected also at Belle II [12]. In particular, in the invisible decay channel, setting new stringent upper limits is already possible with the data collected so far. A full detector simulation of QED backgrounds and signal efficiencies of Belle II was performed in order to determine the sensitivity to dark photons decaying into light DM. Here we assumed the decay width of the A' to be negligible compared to the experimental resolution, and the A' to decay predominantly to dark matter (i.e., the invisible branching fraction is $\sim$100%). The backgrounds for this search are due to high cross section QED processes $e^+e^- \to e^+e^-\gamma(\gamma)$ and $e^+e^- \to \gamma\gamma(\gamma)$ where all but one photon are undetected, being out of the acceptance, or due to gaps or inefficient regions. Therefore, good knowledge of the detector efficiencies is needed for such analysis. Furthermore, this analysis requires the implementation of a dedicated first level (L1) trigger sensitive to single photons. It was not available at the predecessor experiment Belle, and only partially available at the BaBar experiment (BaBar recorded only 53 fb^{-1} of data with the single-photon trigger on). The main difficulty in realizing such a trigger is due to the high rate mainly

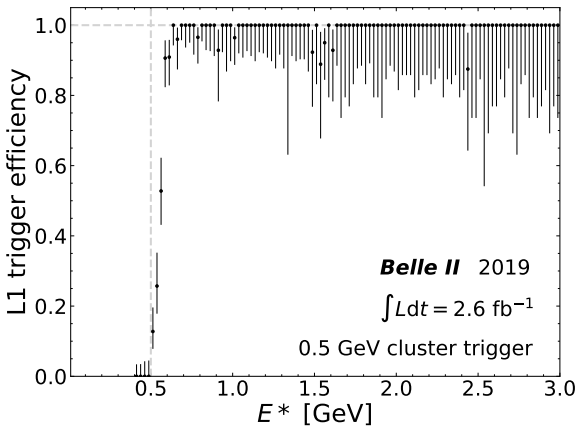

Figure 6: Efficiency of the Level–1 single-photon trigger with a 0.5 GeV threshold as a function of energy measured by using a radiative muon pair sample.

due to radiative Bhabba and $e^+e^- \to \gamma\gamma$ events where only a single photon is produced within the detector acceptance. Belle II has implemented several single-photon trigger lines already from the first operations, with a trigger rate well below the L1 system design maximum output rate of 30 kHz [27]. Remarkably good efficiency values have been measured on the data collected so far, as shown in Figure 6.

The signal selection is done based on the ISR photon energy and polar angle [12]. The expected sensitivities to the mixing parameter ϵ is shown in Figure 7a. With an integrated luminosity of 20 fb^{-1}, Belle II should be able to set a limit considerably lower than the equivalent of BaBar [26]. The better expected sensitivity compared to BaBar is due to the more homogeneous electromagnetic calorimeter of Belle II, whose barrel part has no projective gaps to the interaction point. In BaBar, this caused a large irreducible background of $e^+e^- \to \gamma\gamma(\gamma)$ events, due to one or more photons escaping the detection by passing through projective cracks between adjacent crystals. Additionally, SuperKEKB beam energies provide a smaller boost and larger electromagnetic calorimeter angular coverage, allowing for a larger acceptance of signal events. Furthermore, the Belle II KLM detector can be used to veto photons not detected by the electromagnetic calorimeter.

The sensitivity to high mass is limited by the energy threshold for the single-photon trigger, that has been here conservatively assumed to be 1.8 GeV. However, based on the use of trigger with lower energy thresholds, a significant improvement in sensitivity in the high mass region is expected.

6.1.2. Visible Decay: Analyses of visible decays of the dark photon are also planned. However, these are rather more challenging experimentally as they suffer for high SM backgrounds. Preliminary studies for the visible search at Belle II have been reported in Ref. [12], where the results of the BaBar experiment [22] for the visible decay of an A' via e^+e^- and $\mu^+\mu^-$ final states have been used to extract expected sensitivities. The

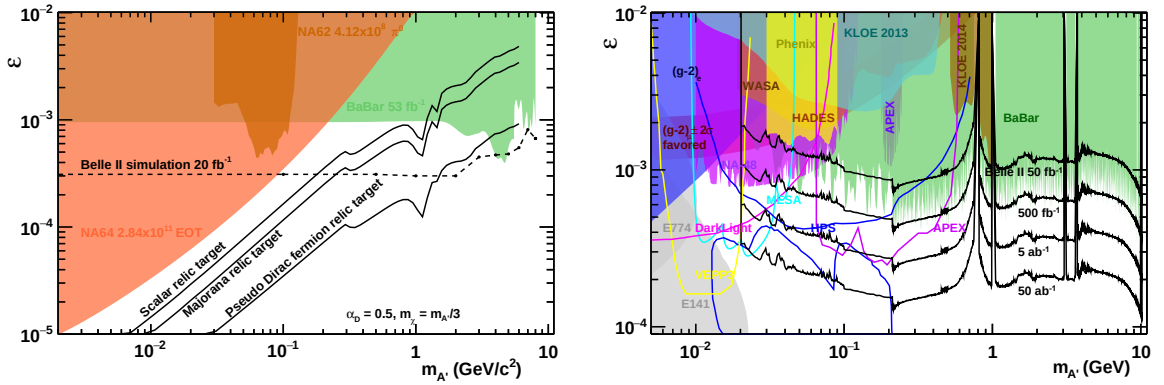

(a) (b)

Figure 7: (a) Expected sensitivity to the kinetic mixing strength for the process $e^+e^- \to \gamma_{\rm ISR}\, A'$, $A' \to \chi\bar{\chi}$ compared to other experiments. (b) Projected limits for Belle 2 on the dark photon kinetic mixing parameter ϵ and mass $m_{A'}$ via the visible decay process $e^+e^- \to \gamma_{\rm ISR}\, A'$, $A' \to l\bar{l}$ compared to other experiments [12].

BaBar analysis is based on a search for a narrow peak in the dilepton mass spectrum on top of a large QED SM background. Taking into account the better invariant mass resolution ($\sim$ a factor 2) of Belle II due to the larger drift chamber radius, as well as a better trigger efficiency for both muons ($\sim$ a factor 1.1) and electrons ($\sim$ a factor 2), the projected sensitivities for different values of integrated luminosity are shown in Figure 7b. Figure7b

Belle II result is expected to be competitive with BaBar once an integrated luminosity of $\mathcal{O}(500)$ fb^{-1} has been accumulated, while with the target luminosity of 50 ab^{-1}, the expectation is to constrain ϵ down to $\mathcal{O}(10^{-4})$

6.2. Dark Higgsstrahlung process

Since the dark photon needs to be massive, one can implement, in close analogy with the SM, a spontaneous breaking mechanism of the U(1) gauge group, introducing a Higgs-like particle h', called *dark Higgs* [28]. The process $e^+e^- \to A'\,h'$, with A' decaying into lepton or hadron pairs, is an interesting reaction to be studied at an e^+e^- collider. The production cross section of the dark Higgsstrahlung process is proportional to the product $\epsilon^2 \times \alpha_{\rm D}$, where $\alpha_{\rm D}$ is the unknown dark coupling constant, and depends on the boson masses [28].

There are two very different scenarios depending on the masses of the dark photon $m_{A'}$ and of the dark Higgs boson $m_{h'}$. For $m_{h'}$ larger than 2 $m_{A'}$, the dark Higgs boson would decay dominantly and promptly to a dark photon pair, thus giving rise to a six charged particle final state. This scenario was investigated by Belle [29] and BaBar [30]. The case with $m_{A'} < m_{h'} < 2m_{A'}$ is similar to the previous, but one dark photon is off shell. On the contrary, if h' is lighter than the dark photon, it would be long-lived for most of the parameter phase space, thus escaping the detection (*invisible dark Higgs*

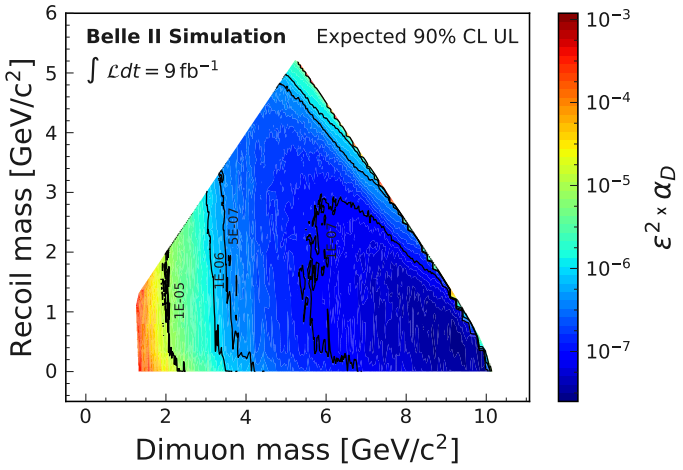

Figure 8: Expected upper limits (90% C.L.) to the coupling constant $\epsilon^2 \times \alpha_D$ for the process $e^+e^- \to A'h'$, $A' \to \mu^+\mu^-$, $h' \to$ invisible, with an integrated luminosity of $9\,\mathrm{fb}^{-1}$, corresponding, roughly, to the 2019 data-taking integrated luminosity.

scenario). This latter case was investigated by the KLOE experiment only, for A' masses up to $\simeq 1$ GeV [31].

6.2.1. Invisible Dark Higgs: Being less constrained, Belle II is planning to search for the A' and h' production into the invisible scenario ($e^+e^- \to A'h'$, $A' \to \mu^+\mu^-$, $h' \to$ invisible) by using data collected during 2019, corresponding to an integrated luminosity of $\sim 9\,\mathrm{fb}^{-1}$. The final state is given by a pair of opposite charge muons plus missing energy. For signal events, the presence of simultaneous peaks both in the distribution of the dimuon invariant mass $M_{\mu\mu}$ and in the distribution of the invariant mass M_{rec} of the system recoiling against the two muons is expected. The interesting phase space region has a triangular shape, being limited on the left by the required condition $M_{\mathrm{rec}} < M_{\mu\mu}$ (being $m_{h'} < m'_A$) and on the right by energy conservation: $M_{\mathrm{rec}} + M_{\mu\mu} < \sqrt{s}$. The measurement is thus performed in the range $2m_\mu < m_{A'} < 10.58$ GeV/c^2 with the constraint $m_{h'} < m_{A'}$, corresponding to a sizeable enlargement of the region explored by KLOE. We expect as main backgrounds the same sources as for the *invisible* Z' analysis, namely $e^+e^- \to \mu^+\mu^-(\gamma)$, $e^+e^- \to \tau^+\tau^-(\gamma)$ and $e^+e^- \to e^+e^-\mu^+\mu^-$, and many of the analysis selections are then very similar. The analysis strategy relies on a mass scan plus counting technique within mass windows of size proportional to the experimental resolution into the two-dimensional mass phase space. Figure 8 shows the expected 90% C.L. upper limits to the coupling constant product $\epsilon^2 \times \alpha_D$. Belle II is expected to constrain $\epsilon^2 \times \alpha_D$ down to $\mathcal{O}(10^{-7})$ in most of the phase space. The sensitivity in the low mass region is limited by the low trigger efficiency due to the low opening angle. In that region, a noticeable improvement is expected with the use of more inclusive triggers available from 2020 on.

7. Conclusions

Although the Belle II experiment is mainly designed to study heavy favour physics, it is expected to be a major player in the search for dark sector particles in the mass range up to $\sim$10 GeV/c^2, thanks to the high luminosity, the improved detector and the specifically designed trigger menus.

In this paper, an overview of the Belle II experiment as well as its capabilities in performing low-mass dark sector searches is given. The first results obtained with the data collected during the 2018 data-taking period have been reviewed, specifically the search for an invisibly decaying Z' (in the framework of the $L_\mu - L_\tau$ model, as well as the model-independent case of a LFV Z') and the search for an ALP decaying into two photons. These results are already state of the art, and will be updated in the future, thanks to the increase in the integrated luminosity and more inclusive trigger lines, which have been recently activated. In addition to the aforementioned searches, the expected sensitivity with the first data has been shown for different searches: ALP decaying invisibly and dark photon searches in radiative processes (both visible and invisible decay channel) and the dark Higgsstrahlung process. However, the landscape of dark sector physics research at Belle II still includes many other studies not mentioned here, such as dark scalars, long-lived particles and magnetic monopoles.

References

[1] Ade P A R *et al.* (Planck) 2016 *Astron. Astrophys.* **594** A13
[2] Essig R, Jaros J A and Wester W 2013 Dark Sectors and New, Light, Weakly-Coupled Particles
[3] Adriani O *et al.* (PAMELA) 2009 *Nature* **458** 607–609
[4] Ackermann M *et al.* (Fermi-LAT) 2012 *Phys. Rev. Lett.* **108** 011103 (*Preprint* `1109.0521`)
[5] Aguilar M *et al.* (AMS) 2013 *Phys. Rev. Lett.* **110**(14) 141102
[6] Bennett G W *et al.* (Muon g-2) 2006 *Phys. Rev. D* **73** 072003 (*Preprint* `hep-ex/0602035`)
[7] Boveia A and Doglioni C 2018 *Ann. Rev. Nucl. Part. Sci.* **68** 429–459 (*Preprint* `1810.12238`)
[8] Essig R, Mardon J, Papucci M, Volansky T and Zhong Y M 2013 *JHEP* **11** 167 (*Preprint* `1309.5084`)
[9] Akai K, Furukawa K and Koiso H 2018 *Nucl. Instrum. Meth. A* **907** 188 – 199
[10] Bona M *et al.* (SuperB) 2007
[11] Abashian A *et al.* (Belle) 2002 *Nucl. Instrum. Meth. A* **479** 117 – 232
[12] Kou E *et al.* (Belle-II) 2019 *PTEP* **2019**
[13] Abudinén F, *et al.* (Belle-II) 2020 *Chinese Physics C* **44** 021001
[14] Jaeckel J and Ringwald A 2010 *Ann. Rev. Nucl. Part. Sci.* **60** 405–437
[15] Peccei R D and Quinn H R 1977 *Phys. Rev. Lett.* **38**(25) 1440–1443
[16] Dolan M, Ferber T, Hearty C, Kahlhoefer F and Schmidt-Hoberg K 2017 *JHEP* **2017**
[17] Abudinén F *et al.* (Belle-II) 2020 *Phys. Rev. Lett.* **125** 161806
[18] Shuve B and Yavin I 2014 *Phys. Rev. D* **89** 113004
[19] Altmannshofer W, Gori S, Profumo S and Queiroz F S 2016 *JHEP* **12** 106
[20] Lees J P, *et al.* (BaBar) 2016 *Phys. Rev. D* **94**(1) 011102
[21] Sirunyan A M *et al.* (CMS) 2019 *Phys. Lett. B* **792** 345–368
[22] Lees J P, *et al.* (BaBar) 2014 *Phys. Rev. Lett.* **113**(20) 201801
[23] Curtin D, Essig R, Gori S and Shelton J 2015 *JHEP* **02** 157
[24] Holdom B 1986 *Phys. Lett. B* **166** 196–198

[25] Pospelov M, Ritz A and Voloshin M B 2008 *Phys. Lett. B* **662** 53–61 (*Preprint* 0711.4866)
[26] Lees J P, *et al.* (BaBar) 2017 *Phys. Rev. Lett.* **119**(13) 131804
[27] Iwasaki Y, Cheon B, Won E, Gao X, Macchiarulo L, Nishimura K and Varner G 2011 *IEEE Trans. Nucl. Sci.* **58** 1807–1815
[28] Batell B, Pospelov M and Ritz A 2009 *Phys. Rev. D* **79** 115008
[29] Jaegle I (Belle) 2015 *Phys. Rev. Lett.* **114** 211801 (*Preprint* 1502.00084)
[30] Lees J *et al.* (BaBar) 2012 *Phys. Rev. Lett.* **108** 211801 (*Preprint* 1202.1313)
[31] Anastasi A *et al.* (KLOE-2) 2015 *Phys. Lett. B* **747** 365–372 (*Preprint* 1501.06795)